LaBH$_8$: the first high-T_c low-pressure superhydride

Simone Di Cataldo,[1, 2, *] Christoph Heil,[1] Wolfgang von der Linden,[1] and Lilia Boeri[2, †]

[1]*Institute of Theoretical and Computational Physics,
Graz University of Technology, NAWI Graz, 8010 Graz, Austria*
[2]*Dipartimento di Fisica, Sapienza Università di Roma, 00185 Roma, Italy*

In the last five years a large number of new high-temperature superconductors have been predicted and experimentally discovered among hydrogen-rich crystals, at pressures which are way too high to meet any practical application. In this work, we report the computational prediction of a hydride superconductor, LaBH$_8$, with a T_c of 126 K at a pressure of 50 GPa, thermodynamically stable above 100 GPa, and dynamically stable down to 40 GPa, an unprecedentedly low pressure for high-T_c hydrides. LaBH$_8$ can be seen as a ternary sodalite-like hydride, in which a metallic hydrogen sublattice is stabilized by the chemical pressure exerted by the guest elements. The combination of two elements with different atomic sizes in LaBH$_8$ realizes a more efficient packing of atoms than in binary sodalite hydrides. A suitable choice of elements may be exploited to further reduce the stabilization pressure to ambient conditions.

The discovery of high-temperature superconductivity (HTSC) at 203 K in sulfur hydride at a pressure of 200 GPa rekindled the dream of achieving room-temperature superconductivity [1–3], triggering a *hydride rush* [4–11] which culminated in the report of superconductivity with a critical temperature (T$_c$) of 287 K (15 °C) at 267 GPa in a carbonaceous sulfur hydride [12]. The first discovery of a room-temperature superconductor set a major milestone in the history of condensed matter physics, but the exceptional pressure required to stabilize the superconducting phase thwarts any practical application.

Obviously, the next challenge for materials research is to find materials exhibiting comparable superconducting properties at, or close to, ambient pressures. Also in this case hydrides, which realize the requirements for conventional HTSC, are a promising hunting ground.

In the five years following the SH$_3$ discovery, all possible combinations of XH$_n$ *binary* hydrides have been computationally explored in an effort to achieve room-temperature superconductivity; these studies revealed that the formation, stability and superconducting properties of these high-pressure (HP) hydrides strongly depend on the ionic size, electronegativity and electronic configuration of the X elements. High-T$_c$ superconductors are found either among *covalent* hydrides, in which X and H form directional bonds driven metallic by pressure, [13–15] or among alkali, alkaline-earth and rare-earth hydrides, which form *sodalite* structures, in which the X atoms do not directly bind to hydrogen but provide a scaffold, that stabilizes a dense sponge-like hydrogen lattice [16–20]. Most HTSC binary hydrides are predicted to be stable above 150-200 GPa; a few are predicted to survive down to 70 GPa, where they are on the verge of a dynamical instability [18, 21]; uranium hydrides are stable above 35 GPa, but do not exhibit HTSC [6, 22].

Having exhausted all possible combinations of binary hydrides, it is natural to extend the search for HTSC to multinary hydrides, where the addition of a third element other than hydrogen, enormously expands the phase space [23, 24]. A few works have already tried to exploit this additional flexibility to to raise the T_c of high-pressure hydrides well beyond room temperature. [25, 26]

In this work, we will demonstrate a strategy to bring the stabilization pressure of high-T_c superconducting hydride phases close to ambient pressure in a ternary hydride. In short, it consists of identifying a suitable combination of elements with different sizes and electronegativity. Our strategy is demonstrated by the prediction of a new ternary high-temperature superconductor, identified through a evolutionary search of the lanthanum-boron-hydrogen (La-B-H) phase diagram [27, 28]. This phase, with LaBH$_8$ composition, exhibits a superconducting T_c of 126 K at 50 GPa. It is a remarkable example of a *ternary sodalite hydride*, in which a cubic La-B scaffolding confines a highly-symmetric, dense hydrogen sublattice, and makes it stable down to moderate pressures. Ternary sodalite hydride phases have been predicted only at pressures above 170 GPa [25, 29], while LaBH$_8$ appears on the ternary La-B-H hull at 110 GPa, and is dynamically stable down to 40 GPa.

The new LaBH$_8$ phase was identified through a structural search at 100 GPa using variable-composition evolutionary crystal structure prediction, as implemented in USPEX [27, 28], by sampling a total of over twelve thousand structures [30]. The ternary La-B-H convex hull was then constructed, including also the zero-point lattice contribution to the total energy. At 100 GPa four stable compositions lie on the convex hull: La(BH$_2$)$_3$, La(BH$_4$)$_3$, LaBH$_5$, and LaBH$_8$. The first two exhibit crystal structures analogous to those observed in other metal borohydrides, i.e. molecular structures with BH$_2^-$ and BH$_4^-$ anions interspaced by La^{3+} cations [24, 31–34], and are insulating. LaBH$_5$ and LaBH$_8$ are characterized by the same La-B rocksalt sublattice. In LaBH$_5$, boron and hydrogen form a BH$_4^-$ tetrahedral anion, and an additional H atom is trapped at the center of a La tetrahedron. For LaBH$_8$ we predict a $Fm\bar{3}m$ sodalite-like
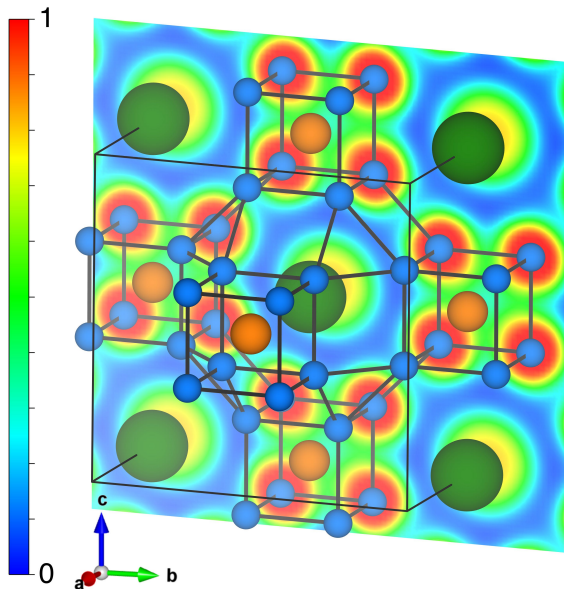
Figure 1. Crystal structure of the $Fm\bar{3}m$ phase of LaBH$_8$ (conventional unit cell). La, B, and H atoms are shown as green, orange, and blue spheres, respectively. The Electron Localization Function (ELF) is projected onto the $\bar{1}00$ plane.

structure. Both LaBH$_5$ and LaBH$_8$ are metallic. Preliminary T_c calculations showed that the LaBH$_5$ structure exhibits a T_c of 53 K at 50 GPa, whereas LaBH$_8$ exhibits a T_c of 126 K at the same pressure [35]. These preliminary results led us to focus on the much more promising LaBH$_8$ $Fm\bar{3}m$ sodalite-like structure.

$Fm\bar{3}m$ LaBH$_8$ lies only 23 meV/atom above the hull at 100 GPa, becomes thermodynamically stable above 110 GPa, and is dynamically stable down to 40 GPa. This implies that this phase can be realistically synthesized by laser heating at 110 GPa, and quenched at low pressures down to a minimum of 40 GPa. The crystal structure of $Fm\bar{3}m$-LaBH$_8$ is shown in Fig. 1: La and B occupy $4b$ and $4a$ Wyckoff positions, respectively, while H atoms sit on $32f$ sites with $x = 0.145$. The hydrogen sites occupy the vertices of a rhombicuboctahedron centered around La atoms, and vertices of cubes around B atoms. Interestingly, a structure with an identical M-B sublattice was observed with neutron diffraction on MBH$_4$ (M = K, Rb, Cs), which only differs by the 1/2 occupancy of the $32f$ site by hydrogen [36].

The Electron Localization Function (ELF) for LaBH$_8$, shown in Fig. 1 along the $\bar{1}00$ plane, has maxima around the atoms, and along the H-H bonds, but not between La and H or B and H, indicating that neither La nor B form bonds with H, but both act as spacers. The absence of a B-H covalent bond is quite unusual for a borohydride, and implies that this structure is not a covalent hydride, like SH$_3$. Rather, it is reminiscent sodalite hydrides like LaH$_{10}$, where a dense, metallic hydrogen sublattice is stabilized at pressures lower than the pure hydrogen at

metallization pressure, due to the chemical pressure exerted by the host atoms. In a very simplified picture, one could see LaBH$_8$ as a chemically-precompressed version of LaH$_{10}$ (for a visual impression see Fig. S3 of the SM [37]). In fact, the two structures share the same La-La sublattice, with almost identical lattice parameters at all pressures; LaH$_{10}$ is stable at the harmonic level only above 200 GPa; in LaBH$_8$, boron atoms fill the voids between the second-nearest La atoms and provide additional chemical pressure, making the metallic hydrogen sublattice stable down to 40 GPa. The analogy of LaBH$_8$ with binary sodalite structures, which is confirmed by the analysis of the electronic structure and vibrational properties, is ultimately at the heart of the HTSC at low pressure. We also observe that at all pressures H-H interatomic distances are 13% larger than sodalite LaH$_6$, and 20% larger than LaH$_{10}$ [18] (see Fig. S5 of the SM [37]). In short, both the geometric and bonding properties indicate that this structure is a natural extension of the concept of *sodalite* hydrides, to the case of a ternary hydride [16, 17].

In Fig. 2 we show the electronic band structure, along with the atom-projected density of states, calculated at 50 GPa. Here and in the following, we will focus on this pressure, which is sufficiently close to the moderate-pressure regime, but is about 10 GPa higher than the dynamical instability pressure, so that predictions are still not dramatically affected by anharmonic effects. A band structure formation analysis (see SM, Fig. S6 [37]) reveals that the eight bands in the -15 to 2 eV range from the Fermi level derive from the eight quasi-free-electron-like bands of the empty H$_8$ sublattice, which are only weakly perturbed by hybridization with the $2s-2p$ boron states, and more strongly by hybridization with the three La semi-core bands from -20 to -15 eV. A Bader charge analysis [38] predicts a net charge of +1.46 for La, +0.88 for B, and -0.29 for each H, indicating that both boron and lanthanum donate charge to the hydrogen sublattice.

Hence, the band structure analysis confirms the bonding picture observed in real space: H forms a dense sublattice, stabilized by the La-B scaffolding with which hydrogen forms only weak bonds. The absence of a covalent B-H bond here is crucial, and explains the free-electron-like behavior of the hydrogen-derived electronic states. In fact, as a result of this weak hybridization electronic bands at the Fermi level are highly-dispersive and have an almost purely (70%) hydrogen character, exactly like binary sodalite hydrides [18].

In the left panel of Fig. 4 we show the Fermi surface decorated with H character. The Fermi surface is characterized by three sheets i) a large electron-like sphere around the Γ point, which has the greatest weight in the reciprocal space, ii) a cross-shaped sheet and a small hole pocket around the X point, mostly of H character, and iii) a small hole pocket around the L point with mixed B and H character. Overall, the whole Fermi surface exhibits a

strong hydrogen character, i.e. the partial H contribution to the DOS is never less than 50 %, on average around 70%.
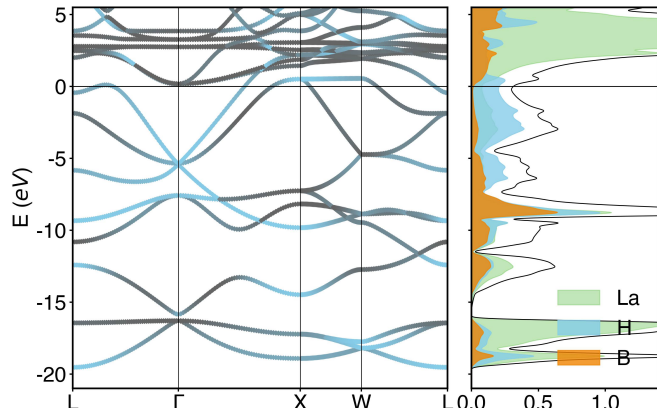

Figure 2. Left panel: electronic band structure of $Fm\bar{3}m$ LaBH$_8$ at 50 GPa, decorated with hydrogen character (blue) vs non-hydrogen character (gray). Right panel: atom-projected density of states in units of eV^{-1}spin^{-1}. Projection onto La, B, and H is shown in green, orange, and blue, respectively. The zero of the energy corresponds to the Fermi level.

In order to compute the superconducting properties of the $Fm\bar{3}m$-LaBH$_8$ phase, we calculated the phonon dispersions and the electron-phonon coupling using linear response theory within the harmonic approximation, using Wannier interpolation on very fine $\vec{k}$ and $\vec{q}$ grids, as implemented in the EPW code [39–41]. In Fig. 3 we show the phonon dispersions decorated with the partial electron-phonon (e-ph) coupling coefficients $\lambda_{\nu\vec{q}}$, together with the atom-projected Eliashberg function $\alpha^2F(\omega)$ and the phonon density of states. The e-ph coupling is spread rather evenly on all optical branches, and is stronger for modes which involve vibrations of the hydrogen sublattice, again in close analogy with other binary sodalite hydrides [18, 42]. The high peak in the Eliashberg function at 50 meV corresponds to a flat region of the dispersion around the Γ point, which experiences a particularly strong e-ph coupling. This phonon mode, named T_{2g}^* in the following, is characterized by a T_{2g} symmetry at the Γ point and corresponds to a distortion of the tetrahedra formed by nearest-neighbours H atoms, and carries around 15% of the total e-ph coupling (See SM Fig. S13 for more details [37]). In addition, a triply degenerate branch with T_{1u} symmetry at Γ, accidentally quasi-degenerate with the T_{2g}^* mode at 50 GPa, is also notable. This branch, in fact, corresponds to a rattling mode of the boron atoms inside the cubic hydrogen cages surrounding it, and is mostly dispersionless throughout the Brillouin zone, coherently with the description of boron as passively pressurizing the metallic hydrogen sublattice, without bonding to it.

Integrating the Eliashberg function we obtain the two moments: [43, 44] $\lambda = 2\int\alpha^2F(\omega)\omega^{-1}d\omega = 1.54$ and $\omega_{\log} = \exp\left[2\lambda^{-1}\int d\omega\alpha^2F(\omega)\omega^{-1}\log(\omega)\right]$ 71 meV. Table I reports the critical temperature obtained by a direct solution of ab-initio Migdal-Eliashberg equations, as implemented in the EPW code [41]. Coulomb effects are included via the Morel-Anderson pseudopotential $\mu^* = \mu/[1 + \mu\log(\omega_{\rm el}/\omega_{\rm ph})]$ [45], with $\omega_{\rm el}$ and $\omega_{\rm ph}$ being characteristic energies for electrons (band-width of the Fermi surface electrons) and phonons (highest phonon energy), respectively. The double Fermi-surface average of the screened Coulomb interaction μ was evaluated within the random phase approximation [46–49]. We find a value of μ^*=0.09 at pressures of 50 and 100 GPa, close to the standard values (0.10-0.14) assumed for most conventional superconductors [18]. This rules out possible anomalous effects of Coulomb repulsion which were suggested for yttrium sodalite hydride [5].

The $T_{\rm c}$ obtained from the fully anisotropic solution ($T_{\rm c}$=126 K) is extremely close to the isotropic one ($T_{\rm c}$=122 K). The anisotropy of the superconducting gap is in fact very limited [50] The distribution of the calculated superconducting gap on the Fermi surface is shown in the right panel of Fig. 4. Indeed, with the exception of a *hotspot* around the X point, which has a negligible weigth in reciprocal space, the gap is rather uniform, with a deviation of ± 15% around its mean value $\Delta_{\rm avg} = 26$ meV. The mean value differs from the isotropic average $\Delta_{\rm iso} = 23.5$ meV, as the isotropic average is affected by the fact that large values of the gap have a small weight in reciprocal space. The calculated BCS parameter $2\Delta_{\rm iso}(0)/T_c$ is 4.3, confirming the strong-coupling nature of superconductivity in LaBH$_8$.
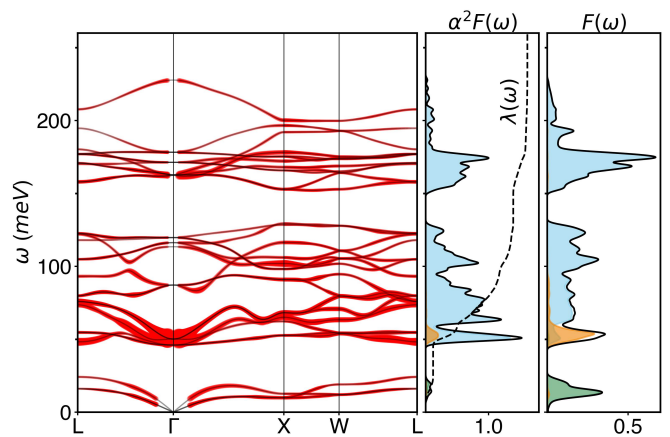

Figure 3. Left panel: phonon dispersions of LaBH$_8$ at 50 GPa (black thin lines), decorated with the e-ph coupling (red thick lines). Center panel: atom-projected (colored filled lines) and total (black line) Eliashberg function, and its first inverse moment $\lambda(\omega)$ (dashed black line). Right panel: atom-projected (colored filled lines) and total (black line) phonon density of states. Projection onto La, B, and H is shown in green, orange, and blue, respectively.

P (GPa)	$N(E_F)$ (eV^{-1})	λ	$\omega_{\log}$ (meV)	T_c^{AME} (K)	T_c^{IME} (K)	Δ_{iso} (meV)	ΔH (meV/at)
50	0.62	1.54	71	126	122	23.5	125
75	0.60	1.06	91	101	96	16.8	71
100	0.56	0.64	88	42	32	5.6	23

Table I. Summary of the main superconducting properties of LaBH$_8$ at 50 and 100 GPa. The DOS at the Fermi level $N(E_F$ in the second column is in units of $eV^{-1}spin^{-1}$. *AME* and *IME* correspond to solutions of the anisotropic and isotropic Migdal-Eliashberg equations, respectively. The T_c is calculated with $\mu^* = 0.09$. Δ_{iso} represents the isotropic average of the superconducting gap. The last column describes the enthalpy per atom (including zero-point energy) above the convex hull for the LaBH$_8$ $Fm\bar{3}m$ phase.
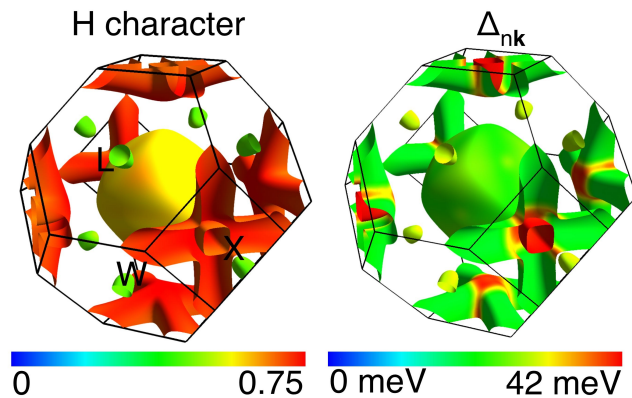

Figure 4. Fermi surface of LaBH$_8$ at 50 GPa. Left: decorated with hydrogen character, right: decorated with the value of the superconducting gap. The color scale goes from zero to the maximum value of the H character (0 to 0.75), and the gap (0 to 42 meV), respectively.

Having established that the superconducting properties of LaBH$_8$ at 50 GPa are extremely promising, we further studied their behavior as a function of pressure, computing the electron-phonon spectra at 75 and 100 GPa, and solving the corresponding Eliashberg equations. The main results are summarized in Tab. I, and more details are provided in SM Fig. S8 [37]. The main effect of an increase in pressure is a rather uniform shift of all phonon frequencies to higher values, which causes a decrease of λ and an increase of ω_{log}. The T_{2g}^* mode around Γ, which at 50 GPa has a frequency of 50 meV, responds more strongly to pressure than the rest of the spectrum, causing a small, counterintuitive decrease of $\omega_{\log}$ between 75 and 100 GPa. The same mode drives the system towards a dynamical instability when pressure is decreased below 50 GPa.

At the harmonic level, the instability occurs at 35 GPa. Vibrations involving hydrogen and, in general, light elements, exhibit strong anharmonic and quantum effects [42, 51], which may severely affect the dynamical stability and/or superconducting properties of hydrides. In

LaBH$_8$, the soft T_{2g}^* mode is also the only strongly anharmonic one. Hence, in order to estimate the importance of anharmonic effects in $Fm\bar{3}m$-LaBH$_8$, We recomputed the frequency of the T_{2g}^* mode, solving the Schrödinger equation numerically as a function of pressure, as described in Ref. [49]. We estimated that the difference between the harmonic and anharmonic frequencies is almost constant with pressure, and equal to $\sim$ 10 meV. This causes a $\sim$ 5 GPa shift of the stability pressure to 40 GPa (See Figs. S11 and S12 of the SM for more details [37]), and a negligible effect on the critical temperature (See Fig. S13 of the SM [37]). The stabilization pressure of LaBH$_8$ represents a new minimum at which a high-T_c superhydride is predicted to be stable, beating the previous record of 70 GPa in YbH$_6$ [21]. We believe that the main reason behind the low stabilization pressure of LaBH$_8$ is *chemical pressure*.

In conclusion, using a evolutionary crystal structure prediction and ab-initio Migdal Eliashberg theory we predicted a new ternary hydride phase with LaBH$_8$ stoichiometry and $Fm\bar{3}m$ space group, which is a conventional HTSC at moderate pressures, with a T_c of 126 K at 50 GPa. According to our estimate, this structure could be synthesized by means of laser heating at a pressure around 100 GPa, and remains dynamically stable down to 40 GPa, where a single zone-center phonon mode drives a structural instability.

LaBH$_8$ is the first conventional superconductor with T_c above liquid nitrogen boiling point that can be stabilized down to 50 GPa. Its exceptional superconducting properties can be understood as deriving from a metallic hydrogen lattice, which is stabilized at low pressures by a boron and lanthanum scaffolding. The combination of two elements with different atomic sizes turns out to be a very effective way to boost chemical pressure on the interstitial hydrogen sublattice. In general, our results demonstrate an effective new strategy to lower the stabilization pressure of binary hydrides. It is likely that the XYH$_8$ $Fm\bar{3}m$ structure may be tuned to attain even better performances, through a careful choice of the X,Y elements. The possibility of stabilizing a superhydride to this pressure represents a giant leap towards hydride-based superconductivity at room pressure.

the useful suggestions and for kindly sharing the code to solve the isotropic Migdal-Eliashberg equations.

———————

* simone.dicataldo@uniroma1.it
† lilia.boeri@uniroma1.it

[1] M. Einaga, M. Sakata, T. Ishikawa, K. Shimizu, M. Eremets, A. P. Drodzov, I. A. Troyan, N. Hirao, and Y. Ohishi, Nature Physics **12**, 835 (2016).

[2] A. P. Drodzov, M. I. Eremets, I. A. Troyan, V. Ksenofontov, and S. I. Shylin, Nature **525**, 73 (2015).

[3] D. Duan, Y. Liu, F. Tian, D. Li, X. Huang, Z. Zhao, H. Yu, B. Liu, W. Tian, and T. Cui, Scientific Reports **4**, 6968 (2014).

[4] P. P. Kong, V. S. Minkov, M. A. Kuzonikov, S. P. Besedin, A. P. Drodzov, S. Mozaffari, L. Balicas, F. F. Balakirev, V. B. Prakapenka, E. Greenberg, D. A. Knyazev, and M. I. Eremets, arXiv:1909.10482 (2019).

[5] I. A. Troyan, D. V. Semenok, A. G. Kvashin, A. V. Sadakov, O. A. Sobolevskiy, V. M. Pudalov, A. G. Ivanova, V. B. Prakapenka, E. Greenberg, A. G. Gavriliuk, V. V. Struzhkin, A. Bergara, I. Errea, R. Bianco, M. Calandra, F. Mauri, L. Monacelli, R. Akashi, and A. R. Oganov, arXiv:1908.01534 (2019).

[6] I. A. Kruglov, A. G. Kvashin, A. F. Goncharov, A. R. Oganov, S. S. Lobanov, N. Holtgrewe, S. Jiang, V. B. Prakapenka, E. Greenberg, and A. V. Yanilkin, Science Advances **4** (2018).

[7] D. V. Semenok, A. G. Kvashin, A. G. Ivanova, V. Svitlyk, V. Y. Fominski, A. V. Sadakov, O. A. Sobolevskiy, V. M. Pudalov, I. A. Troyan, and A. R. Oganov, Materials Today **33**, 36 (2020).

[8] A. P. Drodzov, M. I. Eremets, and I. A. Troyan, arXiv:1508.06224 (2015).

[9] A. P. Drodzov, P. P. Kong, S. P. Besedin, M. A. Kuzonikov, S. Mozaffari, L. Balicas, F. F. Balakirev, D. E. Graf, V. B. Prakapenka, E. Greenberg, D. A. Knyazev, M. Tkacz, and M. I. Eremets, Nature **569**, 528 (2019).

[10] M. Somayazulu, M. Ahart, A. K. Mishra, Z. M. Geballe, M. Baldini, Y. Meng, V. V. Struzhkin, and R. J. Hemley, Phys. Rev. Lett. **122**, 027001 (2019).

[11] J. A. Flores-Livas, L. Boeri, A. Sanna, G. Profeta, R. Arita, and M. Eremets, Physics Reports **856**, 1 (2020).

[12] E. Snider, N. Dasenbrock-Gammon, R. McBride, M. Debessai, H. Vindana, K. Vencatasamy, K. V. Lawler, A. Salamat, and R. P. Dias, Nature **586**, 373 (2020).

[13] J. A. Flores-Livas, M. Amsler, C. Heil, A. Sanna, L. Boeri, G. Profeta, C. Wolverton, S. Goedecker, and E. K. U. Gross, Phys. Rev. B **93**, 020508 (2016).

[14] N. Bernstein, C. S. Hellberg, M. D. Johannes, and I. I. Mazin, Phys. Rev. B **91** (2015).

[15] C. Heil and L. Boeri, Phys. Rev. B **92**, 060508(R) (2015).

[16] H. Wang, J. S. Tse, K. Tanaka, T. Iitaka, and Y. Ma, PNAS **109**, 6463 (2012).

[17] F. Peng, Y. Sun, C. J. Pickard, R. J. Needs, Q. Wu, and Y. Ma, Phys. Rev. Lett. **119**, 107001 (2017).

[18] C. Heil, S. Di Cataldo, G. B. Bachelet, and L. Boeri, Phys. Rev. B **99**, 220502(R) (2019).

[19] Y. Sun and M. Miao, Preprint available (v1) at Research Square 10.21203/rs.3.rs-130093/v1 (2021).

[20] S. Yi, C. Wang, H. Jeon, and J.-H. Cho, Phys. Rev. M **5**, 024801 (2021).

[21] H. Song, Z. Zhang, T. Cui2, C. J. Pickard, V. Z. Kresin, and D. Duan, arXiv:2010.12225 (2020).

[22] B. Guigue, A. Marizy, and P. Loubeyre, Phys. Rev. B **102**, 014107 (2020).

[23] C. Kokail, W. von der Linden, and L. Boeri, Phys. Rev. M **1**, 074803 (2017).

[24] S. Di Cataldo, W. von der Linden, and L. Boeri, Phys. Rev. B **102**, 014516 (2020).

[25] Y. Sun, J. Lv, Y. Xie, H. Liu, and Y. Ma, Phys. Rev. Lett. **123**, 097001 (2019).

[26] D. V. Semenok, I. A. Troyan, A. G. Kvashin, A. G. Ivanova, M. Hanfland, A. V. Sadakov, O. A. Sobolevskiy, K. S. Pervakov, A. G. Gavriliuk, I. S. Lyubutin, K. V. Glazyrin, N. Giordano, D. N. Karimov, A. B. Vasiliev, R. Akashi, V. M. Pudalov, and A. R. Oganov, arXiv:2012.04787 (2020).

[27] C. W. Glass, A. R. Oganov, and N. Hansen, Computer Physics Communication **175**, 713 (2006).

[28] A. O. Lyakhov, A. R. Oganov, H. T. Stokes, and Q. Zhu, Computer Physics Communication **184**, 1172 (2013).

[29] X. Liang, A. Bergara, L. Wang, B. Wen, Z. Zhao, X.-F. Zhou, J. He, G. Gao, and Y. Tian, Phys. Rev. B **99**, 100505(R) (2019).

[30] In addition, we re-sampled particularly promising compositions. Further details are provided in the Supplemental Material [37].

[31] M. Paskevicius, L. H. Jepsen, P. Schouwink, R. Cerný, D. B. Ravnsbaek, Y. Filinchuk, M. Dornheim, F. Besenbacher, and T. R. Jensen, Chem. Soc. Rev. **46**, 1565 (2017).

[32] Y. Zhang, E. Majzoub., V. Ozolins, and C. Wolverton, Phys. Rev. B **82**, 174107 (2010).

[33] J. B. Grinderslev, M. B. Ley, Y.-S. Lee, L. H. Jepsen, M. J. rgensen, Y. W. Cho, J. rgen Skibsted, and T. R. Jensen, Inorganic Chemistry **59**, 7768 (2020).

[34] L. H. Rude, T. K. Nielsen, D. B. Ravnsbaek, U. Bösenberg, M. B. Ley, B. Richter, L. M. Arnbjerg, M. Dornheim, Y. Filinchuk, F. Besenbacher, and T. R. Jensen, Phys. Status Solidi **208**, 1754 (2011).

[35] Additional information on the crystal structures can be found in the form of Crystallographic Information File in the Supplemental Material [37].

[36] G. Renaudin, S. Gomes, H. Hagemann, L. Keller, and K. Yvon, Journal of Alloys and Compounds **375**, 98 (2004).

[37] The Supplemental Material is available at..

[38] E. Sanville, S. D. Kenny, R. Smith, and G. Henkelmann, J. Comp. Chem. **28**, 899 (2007).

[39] S. Baroni, S. de Gironcoli, A. D. Corso, and P. Giannozzi, Rev. Mod. Phys **73**, 515 (2001).

[40] S. Y. Savrasov and D. Y. Savrasov, Phys. Rev. B **54**, 16487 (1996).

[41] S. P. and E. R. Margine, C. Verdi, and F. Giustino, Comp. Phys. Communications **209**, 116 (2016).

[42] I. Errea, F. Belli, L. Monacelli, A. Sanna, T. Koretsune, T. Tadano, R. Bianco, M. Calandra, R. Arita, F. Mauri, and J. A. Flores-Livas, Nature **578**, 66 (2020).

[43] W. L. McMillan, Physical Review **167**, 331 (1968).

[44] P. B. Allen and R. C. Dynes, Phys. Rev. B **12**, 905 (1975).

[45] P. Morel and P. W. Anderson, Physical Review **125**, 1263 (1962).

[46] K.-H. Lee, K. J. Chang, and M. L. Cohen, Phys. Rev. B **52**, 1425 (1995).

[47] F. Giustino, M. L. Cohen, and S. G. Louie, Phys. Rev. B **81**, 115105 (2010).

[48] H. Lambert and F. Giustino, Phys. Rev. B **88**, 075117 (2013).

[49] C. Heil, S. Poncé, H. Lambert, M. Schlipf, E. R. Margine, and F. Giustino, Phys. Rev. Lett. **119**, 087003 (2017).

[50] We also checked the dependence of μ^* on Tc and found that a variation of 0.01 in μ^* changes Tc only by 2-3 K (See SM Fig. S9 for more details [37])

[51] I. Errea, M. Calandra, C. J. Pickard, J. R. Nelson, R. J. Needs, Y. Li, H. Liu, Y. Zhang, Y. Ma, and F. Mauri, Nature **532**, 81 (2016).